SUPPORTING INFORMATION

Optimization of Carbonization and Composition in FeCC Composites for Enhanced Lithium-Ion Battery Anode Performance

Do Thao Anh[a,b], Nguyen Bao Tran[b,c], Quang Ngoc Tran[a,b], Hanh Kieu Thi Ta[a,b,c], Bach Thang Phan[a,b,d], Tuan Loi Nguyen[e,f], Nhu Hoa Thi Tran[b,c,*]

[a.] *Advanced Materials Technology Institute Vietnam National University Ho Chi Minh city (formerly affiliated with Center for Innovative Materials and Architectures), Ho Chi Minh City, Viet Nam*
[b.] *Viet Nam National University, Ho Chi Minh City, Viet Nam*
[c.] *Faculty of Materials Science and Technology, University of Science, Ho Chi Minh City, Vietnam*
[d.] *University of Health Sciences, Vietnam National University Ho Chi Minh City, Viet Nam*
[e.] *Institute of Fundamental and Applied Sciences, Duy Tan University, Ho Chi Minh City, Vietnam*
[f.] *Faculty of Environmental and Chemical Engineering, Duy Tan University, Da Nang City, Vietnam*

* Corresponding author: Nhu Hoa Thi Tran (Email: ttnhoa@hcmus.edu.vn)

Chemical and reagent. Cobaltous nitrate ($Co(NO_3)_2.6H_2O$, $\geq$ 98%), 2-methylimidazole ($C_4H_6N_2$, Hmim, 99 %), polyvinylpyrrolidone ($(C_6H_9NO)_n$, PVP, Mw ~ 55.000), sodium citrate tribasic dihydrate ($C_6H_5Na_3O_7.2H_2O$, 99 %), ammonium hydroxide (NH_4OH, 30% NH_3 basic), ferrous chloride tetrahydrate ($FeCl_2.4H_2O$, 99.9 %), ferric chloride hexahydrate ($FeCl_3.6H_2O$, 97 %), super P (C, 99 %), polyvinylidene fluoride (PVDF, Mw ~ 534.000), and 1-Methyl-2-pyrrolidone (NMP, 99 %) were all purchased from Sigma-Aldrich Inc. (St. Louis, MO, USA). De-ionized (DI) water (Thermo Scientific Easypure II, Göteborg, Sweden), produced at the Center for Innovative Materials and Architectures (INOMAR), Vietnam National University, Ho Chi Minh City (VNU-HCM), was utilized for all sample preparations.

Material characterization. Powder X-ray diffraction (PXRD, Bruker D8 Advance diffractometer, λ is 1.54178 Å) and Fourier-transform infrared spectroscopy (FTIR, Bruker Vertex 70) were used to analyze the crystal structure and the composition and chemical functions of the samples. Field emission scanning electron microscope (FESEM, Hitachi S4800, USA) operated at an accelerating voltage of 5 kV and an energy dispersive X-ray spectroscope (EDS) installed in the equipment. High-resolution TEM (HR-TEM) images were obtained using a JEM-ARM200F (JEOL) instrument. Further, the structural features were examined using X-ray photoelectron spectroscopic (XPS) measurements.

Electrochemical measurements. Galvanostatic charge-discharge (GCD) cycling was conducted at a constant current density of 100 mA g^{-1} over a potential window of 0.01 – 3.00 V (vs Li/Li^+) using a battery cycler system (NEWARE). Electrochemical impedance spectroscopy (EIS) was carried out using a Gamry (1010E) across frequencies ranging from 100 kHz to 100 mHz. Cyclic voltammetry (CV) was also performed at scan rates of 0.3 – 1.2 mV s^{-1} over 0.01 – 3.00 V (vs Li/Li^+) on Arbin instrument. The CV response of the anode provided insights into the lithiation/delithiation kinetics and facilitated analysis of the reaction kinetics at the anode electrode.

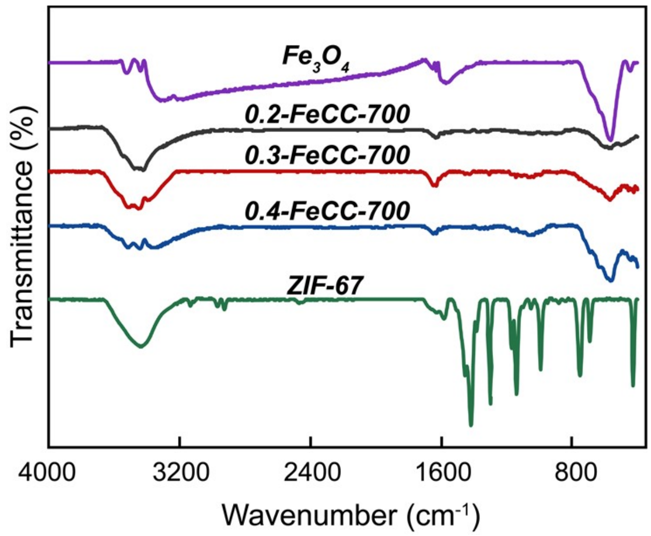

Figure S1. FTIR specta of Fe_3O_4, ZIF-67, 0.2-FeCC-700, 0.3-FeCC-700 and 0.4-FeCC-700 samples.

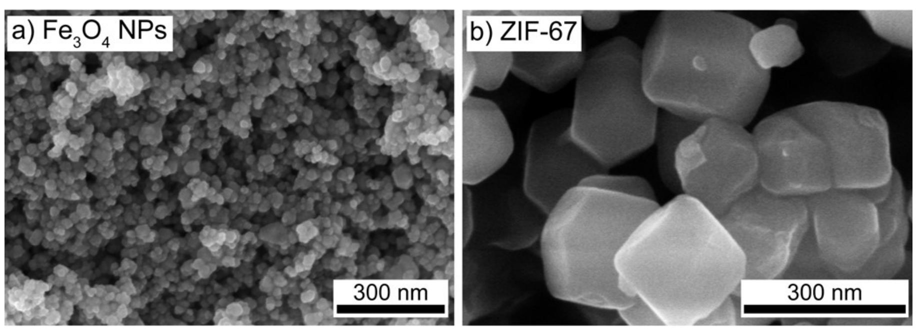

Figure S2. FESEM images of (a) Fe_3O_4 NPs and (b) ZIF-67 rhombic dodecahedron.

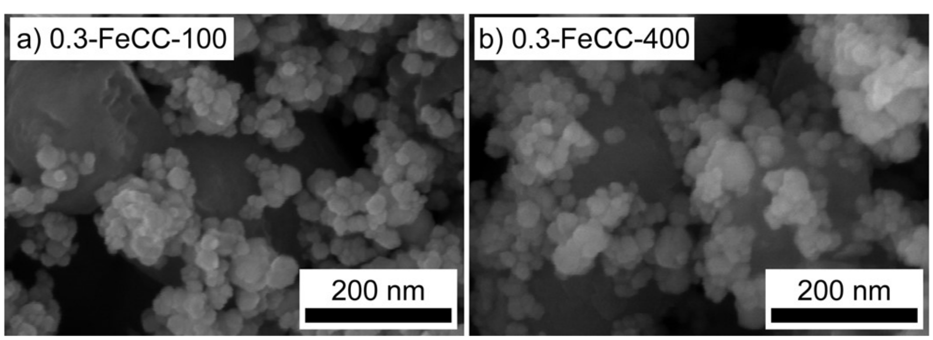

Figure S3. FESEM images of (a) 0.3-FeCC-100; (b) 0.3- FeCC-400 hybrid composite.

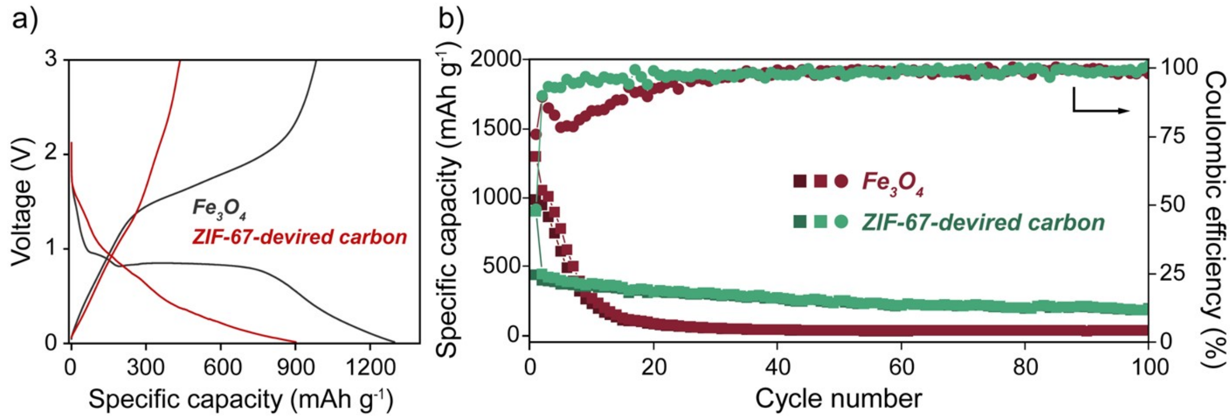

Figure S4. (a) Galvanostatic charge/discharge curves at first cycle; (b) Coulombic efficiency of Fe_3O_4 and ZIF-67-derived carbon anode electrodes.

Table S1. Cycling performance of Fe-based or MOF-derived anode electrodes previously reported.

Anode material	Cycling performance	Current density	Cycle number	Ref
Hybrid nanoporous carbons (HPCs)	332 mAh g^{-1}	50 mA g^{-1}	100	[1]
α-Fe_2O_3@Fe_3O_4 on carbon fiber fabric	328.6 mAh g^{-1}	25 mA g^{-1}	100	[2]
CoP	191 mAh g^{-1}	100 mA g^{-1}	100	[3]
NC-ZIF	279.73 mAh g^{-1}	200 mA g^{-1}	100	[4]
Fe-Co-700	~ 400 mAh g^{-1}	500 mA g^{-1}	100	[5]
FeS_2	61 mA h g^{-1}	100 mA g^{-1}	100	[6]
Sn/C	310.6 mAh g^{-1}	100 mA g^{-1}	300	[7]
Co-TBA	433.9 mAh g^{-1}	100 mA g^{-1}	100	[8]
0.2-FeCC-700 0.3-FeCC-700 0.4-FeCC-700	256 mAh g^{-1} 447 mAh g^{-1} 344 mAh g^{-1}	100 mA g^{-1}	80	**This work**

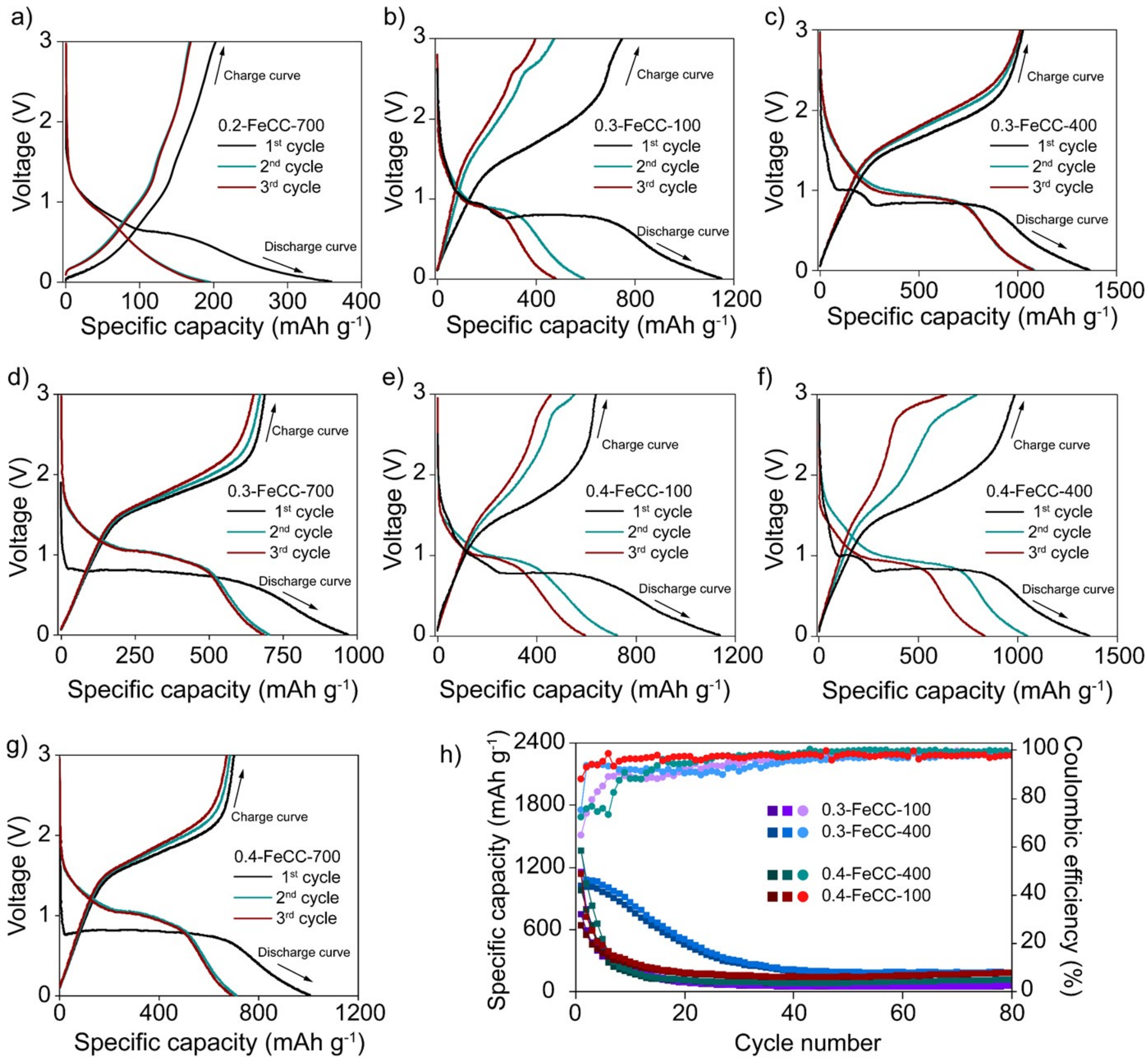

Figure S5. (a-g) The galvanostatic charge/discharge curves of *x*-FeCC-*y* anode electrodes under the first three cycles and (h) Coulombic efficiency of 0.3-FeCC-100, 0.3-FeCC-400, 0.4-FeCC-100 and 0.4-FeCC-400 anode electrodes.

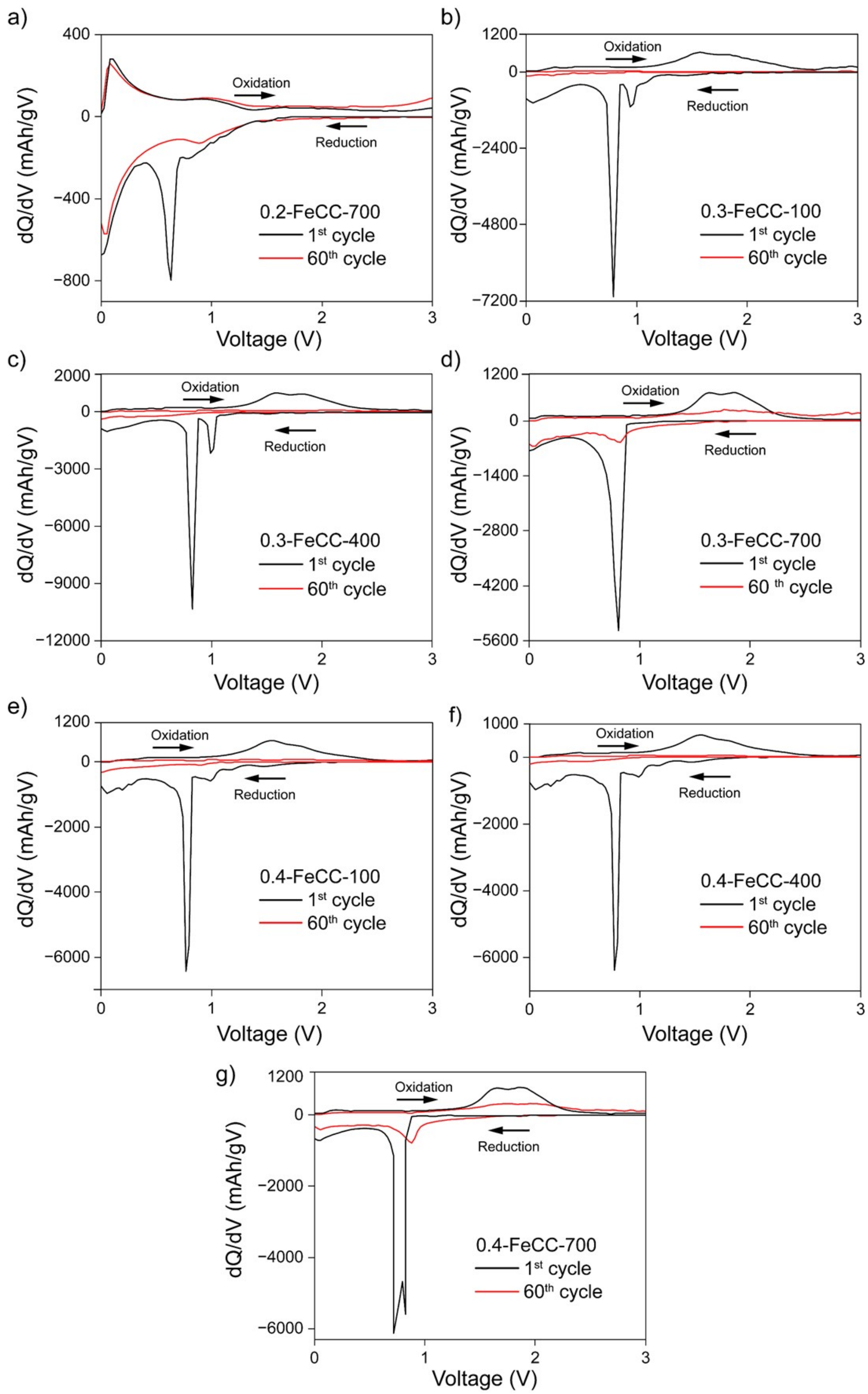

Figure S6. Differential capacity (dQ/dV) plots of the 1st and 60th cycles for the x-FeCC-y anode electrode.

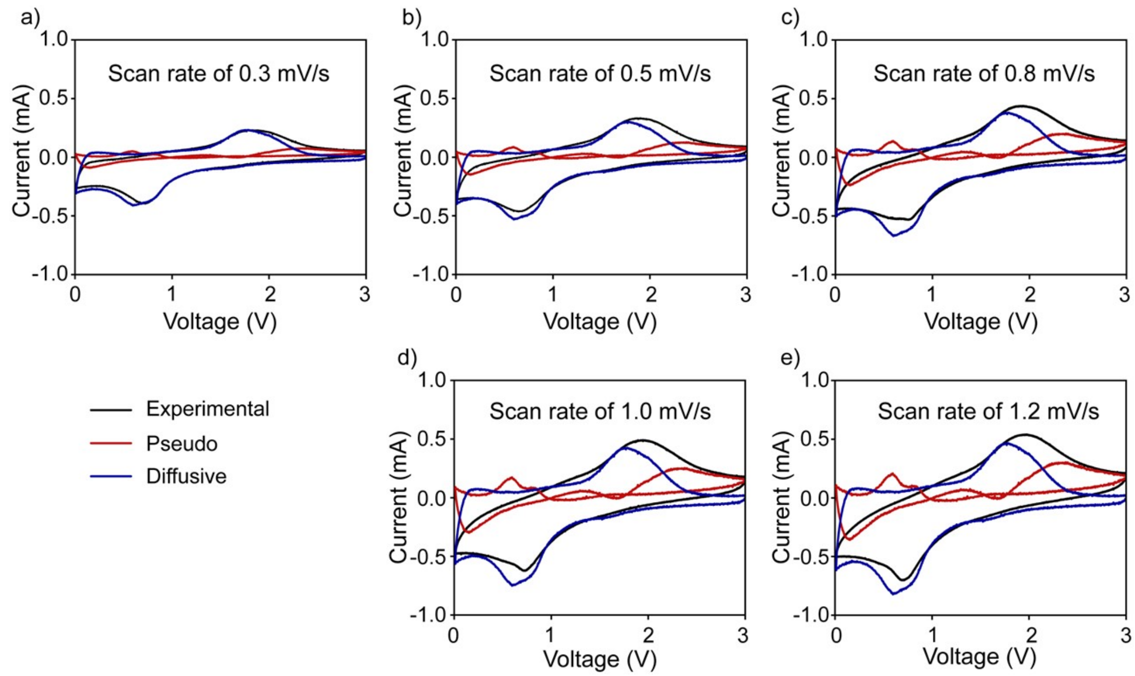

Figure S7. (a – e) Details of pseudo and diffusive curves at various scan rates of 0.3-FeCC-700 electrode.

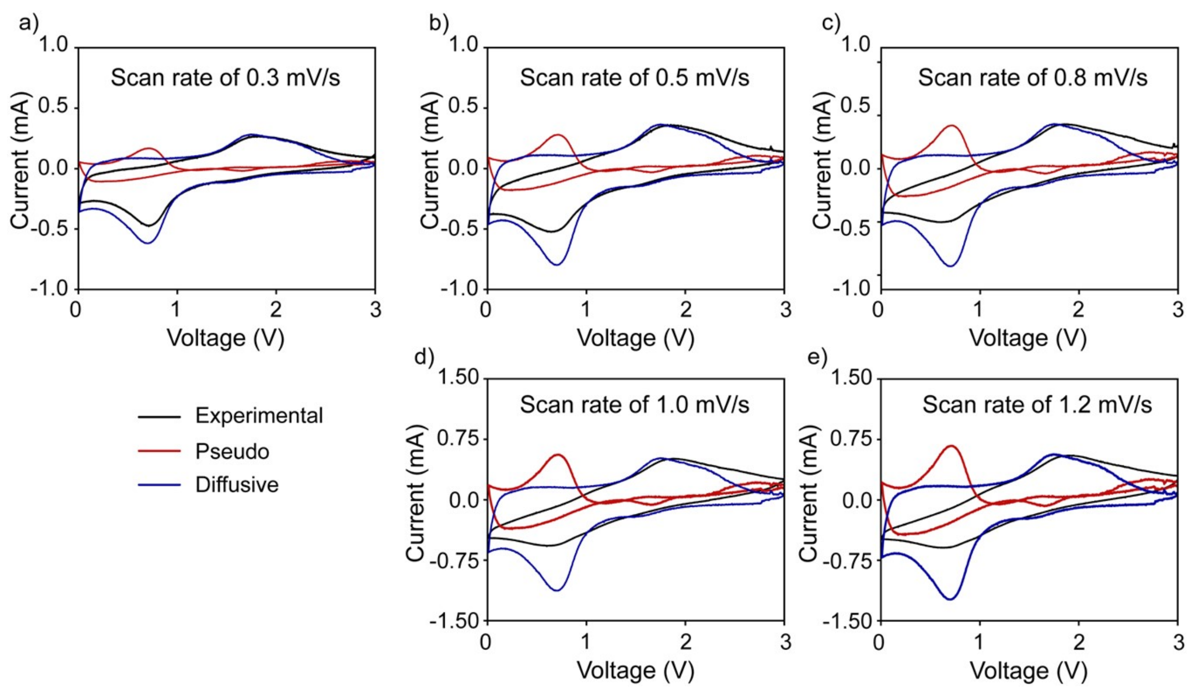

Figure S8. (a – e) Details of pseudo and diffusive curves at various scan rates of 0.4-FeCC-700 electrode.

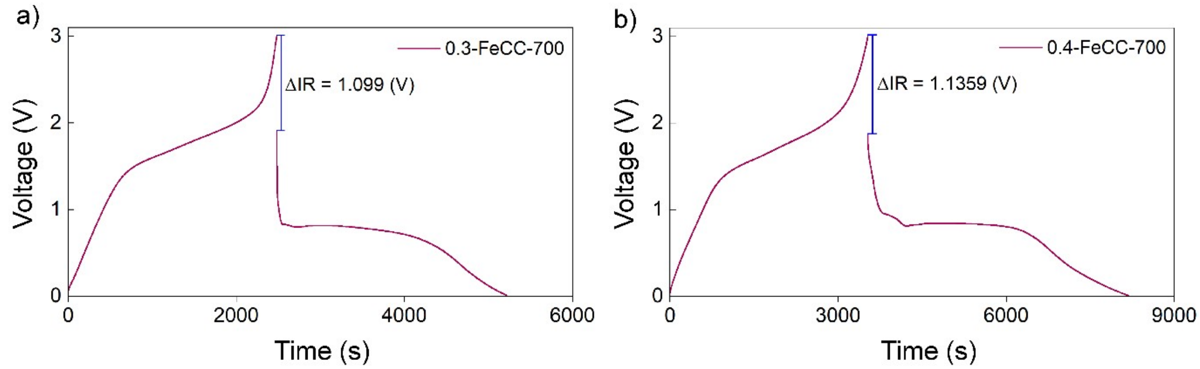

Figure S9. Illustration of the potential drop in the interval between charge and discharge of (a) 0.3-FeCC-700 and (b) 0.4-FeCC-700 electrodes.

Table S2. The potential values corresponding to the oxidation and reduction peaks in the third-cycle CV curves at a scan rate of 0.3 mV s^{-1} for the 0.3-FeCC-700 and 0.4-FeCC-700 electrodes.

Anode electrode	$E_{p\text{-}anodic}$ **(V)**	$E_{p\text{-}cathodic}$ **(V)**	ΔE_p **(V)**
0.3-FeCC-700	1.94	0.86	1.08
0.4-FeCC-700	1.98	0.85	1.13
$E_{p\text{-}anodic}$ *is the potential value (V) at the oxidation peak of the CV curve.* $E_{p\text{-}cathodic}$ *is the potential value (V) at the reduction peak of the CV curve.*			

References

[1] M. Guo, T. Gao, H. Ma, H. Li, Weaving ZIF-67 by employing carbon nanotubes to constitute hybrid anode for lithium ions battery, Mater Lett 212 (2018) 143–146. https://doi.org/10.1016/J.MATLET.2017.10.091.

[2] A. González-Banciella, D. Martinez-Diaz, J. de Prado, M.V. Utrilla, M. Sánchez, A. Ureña, MOF-derived α-Fe_2O_3@Fe_3O_4 on carbon fiber fabric for lithium-ion anode applications, J Energy Storage 90 (2024) 111904. https://doi.org/10.1016/J.EST.2024.111904.

[3] Y. Liu, X. Que, X. Wu, Q. Yuan, H. Wang, J. Wu, Y. Gui, W. Gan, ZIF-67 derived carbon wrapped discontinuous CoxP nanotube as anode material in high-performance Li-ion battery, Mater Today Chem 17 (2020) 100284. https://doi.org/10.1016/J.MTCHEM.2020.100284.

[4] M. Wang, F. Xi, S. Li, W. Ma, X. Wan, Z. Tong, B. Luo, ZIF-67-derived porous nitrogen-doped carbon shell encapsulates photovoltaic silicon cutting waste as anode in high-performance lithium-ion batteries, Journal of Electroanalytical Chemistry 931 (2023) 117210. https://doi.org/10.1016/J.JELECHEM.2023.117210.

[5] X.-N. Lv, P.-F. Wang, Y.-H. Zhang, Q. Shi, F.-N. Shi, MOF-derived $CoFe_2O_4$/FeO/Fe nanocomposites as anode materials for high-performance lithium-ion batteries, J Alloys Compd 923 (2022) 166316. https://doi.org/10.1016/j.jallcom.2022.166316.

[6] W. Yin, W. Li, K. Wang, W. Chai, W. Ye, Y. Rui, B. Tang, FeS_2@Porous octahedral carbon derived from metal-organic framework as a stable and high capacity anode for lithium-ion batteries, Electrochim Acta 318 (2019) 673–682. https://doi.org/10.1016/J.ELECTACTA.2019.05.152.

[7] Y. Cui, Z. Xu, H. Qiu, D. Jin, Enhanced cycling stability of lithium-ion batteries with Sn-MOF derived Sn anodes encapsulated within a three-dimensional carbon framework, Solid State Sci 163 (2025) 107920. https://doi.org/10.1016/J.SOLIDSTATESCIENCES.2025.107920.

[8] L. Wang, J. Chen, H. Yang, H. Dong, Y. Yu, J. Sun, J. Sha, Co_3O_4@C nanocomposites derived from the thermal decomposition of Co-based metal-organic frameworks for lithium

storage, J Solid State Chem 345 (2025) 125239. https://doi.org/10.1016/J.JSSC.2025.125239.